Research Square

Preprints are preliminary reports that have not undergone peer review.
They should not be considered conclusive, used to inform clinical practice,
or referenced by the media as validated information.

Citrate-Tuned Au/Hydroxyapatite for Solvent-Free Aerobic Oxidation of Benzyl Alcohol

Afef Mehri

mehri.afef@yahoo.fr

University of Monastir

Mohamed Hassen Baouab

University of Monastir Institute of Preparatory Studies in Engineering of Monastir

Research Article

Keywords: Citrate-functionalization, apatite, gold nanoparticles, green oxidation, Reusability

Posted Date: September 29th, 2026

DOI: https://doi.org/10.21203/rs.3.rs-11089260/v1

License: This work is licensed under a Creative Commons Attribution 4.0 International License.
Read Full License

Additional Declarations: No competing interests reported.

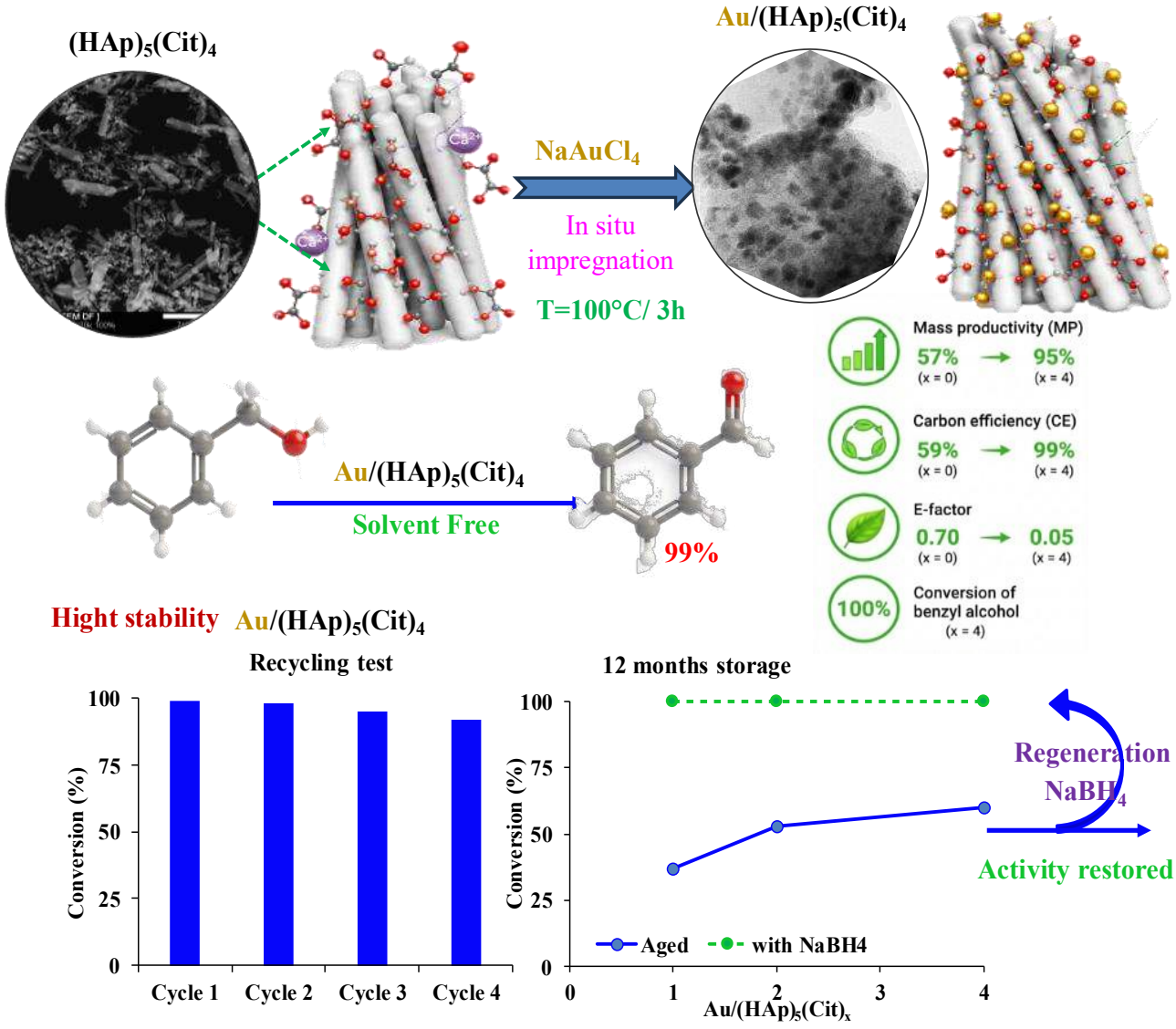
Citrate-Tuned Au/Hydroxyapatite for Solvent-Free Aerobic Oxidation of Benzyl Alcohol

Afef Mehri [a,*], Mohamed Hassen V. Baouab[a]

[a]*Laboratory of Physico-Chemistry of Innovative Materials, LR24ES16, Preparatory Institute for Engineering Studies of Monastir, University of Monastir, Avenue of the Environment 5000, Monastir, Tunisia*

***Corresponding author: E-Mail address:** mehri.afef@yahoo.fr

Graphical abstract



Abstract

Engineering metal–support interfaces through controlled surface functionalization offers a versatile route to tailor supported metal catalysts. Here, citrate-functionalized hydroxyapatite (HAp) serves as an inorganic–organic platform for the in-situ formation of Au nanoparticles, evaluated in the solvent-free aerobic oxidation of benzyl alcohol. A series of $Au/(HAp)_5(Cit)_x$ catalysts (x = 0, 1, 2, 4) was prepared to correlate citrate loading with surface properties, Au dispersion, and catalytic performance. Multi-technique characterization (XRD, ATR-FTIR, N_2 physisorption, XPS, SEM-EDX, HR-TEM, ICP-OES) reveals that citrate functionalization tunes HAp surface chemistry and texture while promoting a more homogeneous distribution of Au nanoparticles. Increasing citrate content modifies the electronic environment of surface Au, as evidenced by shifts in Au 4f binding energies and changes in the Au/Ca surface ratio. Catalytic activity increases with citrate loading, with $Au/(HAp)_5(Cit)_4$ achieving 99% benzyl alcohol conversion under solvent-free conditions using O_2. This performance is accompanied by high process efficiency (95% mass productivity, E-factor 0.05, 99% carbon efficiency). Prolonged reaction times favor over-oxidation to benzoic acid, highlighting the activity–selectivity trade-off. The catalysts show good recyclability; long-term storage induces partial oxidation and restructuring of surface Au, but $NaBH_4$ treatment substantially restores activity. These results establish citrate functionalization as an effective strategy to modulate Au–HAp interfacial properties and define structure–activity relationships for aerobic alcohol oxidation.

Keywords: Citrate-functionalization, apatite, gold nanoparticles, green oxidation, Reusability

1. Introduction

The selective aerobic oxidation of alcohols into value-added oxygenated compounds represents a fundamental challenge in sustainable catalysis, as it enables the replacement of stoichiometric oxidants by molecular oxygen while reducing waste generation and improving atom efficiency[1–3]. Benzyl alcohol oxidation represents an important transformation in sustainable fine chemical synthesis, enabling the production of high-value oxygenated compounds such as benzaldehyde and benzoic acid [4–6]. Benzaldehyde is a key intermediate in the preparation of pharmaceuticals, heterocyclic compounds, fragrances, and chiral building blocks, owing to the versatile reactivity of its aldehyde functionality [7–9]. Benzoic acid, in turn, serves as an essential precursor for pharmaceutical ingredients, antifungal compounds, and industrial preservatives [10, 11]. However, achieving controlled oxidation pathways remains challenging because benzaldehyde, once formed, can undergo further oxidation to benzoic acid under aerobic conditions. Therefore, precise regulation of oxygen activation and surface reaction intermediates is required to selectively direct the reaction toward the desired product. Hence, the development of selective catalytic systems enabling tailored oxidation toward benzaldehyde or benzoic acid under mild and sustainable conditions is of great relevance to the pharmaceutical and specialty chemical industries [12].

Among noble metal-based catalysts, supported gold nanoparticles have demonstrated remarkable potential for aerobic oxidation reactions due to their ability to activate molecular oxygen under relatively mild conditions while exhibiting high resistance toward overoxidation compared with conventional transition-metal catalysts [13, 14]. Nevertheless, the catalytic performance of Au-based systems is intrinsically dependent on nanoscale parameters, including particle size, dispersion, oxidation state, electronic properties, and the nature of the metal–support interface [14, 15] .

While conventional oxide supports have been extensively investigated, surface functionalization strategies have recently emerged as powerful tools to regulate precursor anchoring, nanoparticle nucleation and growth, and the electronic structure of supported metal species through molecular-level engineering of metal–support interfaces[16–18]. Organic surface modifiers containing oxygenated functionalities can provide selective coordination sites for metal precursors, improve nanoparticle stabilization, and modify the local electronic environment of active metal sites. However, achieving an optimal balance between nanoparticle confinement, accessibility of active sites, and preservation of catalytic interfaces remains a significant challenge.

Hydroxyapatite (HAp, $Ca_{10}(PO_4)_6(OH)_2$), a calcium phosphate mineral structurally analogous to biological apatite, has attracted interest as a catalytic support owing to its tunable acid–base properties, ion-exchange capability, and the presence of surface Ca^{2+} and phosphate groups that can participate in the anchoring of metal species and organic modifiers [19, 20]. In particular, citrate molecules, owing to their multiple carboxylate groups, can strongly coordinate surface calcium sites, offering a versatile route for modifying HAp surface properties and controlling noble metal deposition [21–23]. Although citrate is extensively used as a stabilizing ligand during colloidal nanoparticle synthesis, its role as a surface engineering agent for regulating metal nucleation, interfacial electronic properties, and catalytic behavior on inorganic supports remains poorly understood. Establishing clear correlations between citrate-induced surface modification, Au nanoparticle characteristics, and catalytic performance is therefore essential for the rational design of advanced supported gold catalysts.

In this work, citrate-functionalized hydroxyapatite was employed as a tailored platform for controlling the formation and catalytic properties of gold nanoparticles in the solvent-free aerobic oxidation of benzyl alcohol. A series of $Au/(HAp)_5(Cit)_x$ catalysts with controlled citrate contents was synthesized through an in-situ deposition approach. Comprehensive structural, spectroscopic, and microscopic investigations combined with catalytic evaluation were performed to elucidate the influence of citrate-mediated surface engineering on Au nanoparticle dispersion, metal–support interactions, oxygen activation, and oxidation selectivity. The obtained insights provide fundamental understanding of the role of organic–inorganic interfaces in designing efficient and sustainable gold-based oxidation catalysts.

2. Materials and methods

2.1 Chemical reagents

Citric acid ($C_6H_8O_7$, 99%) and tetrachloroauric (III) sodium dihydrate ($NaAuCl_4.2H_2O$, 99%) were obtained from Sigma Aldrich. Calcium nitrate ($Ca(NO_3)_2.4H_2O$, 99%) and diammonium hydrogen orthophosphate ($(NH_4)_2HPO_4$, 99%) were supplied by Merck. Benzyl alcohol (99.8%), benzaldehyde (C_6H_5CHO, 99%) and benzoic acid (99.5%) were obtained from Sigma-Aldrich. All the chemicals were of analytical reagent (AR) grade and were used without further purification.

2.2 Functionalization of hydroxyapatite surface

Citrate-functionalized hydroxyapatite nanopowders were prepared through a modified co-precipitation route according to a previously reported procedure [24]: Briefly, a calculated amount of citric acid was introduced into an aqueous calcium nitrate solution (5.0×10^{-2} mol

L^{-1}) to obtain Cit/Ca molar ratios of x = 1, 2, and 4. The pH of the solution was maintained at 11 by the controlled addition of ammonium hydroxide solution (NH_4OH, 28 wt%). After 30 min of vigorous stirring, an aqueous diammonium hydrogen phosphate solution was added dropwise at a controlled rate of 1 mL min^{-1} while maintaining the Ca/P molar ratio at 1.67. The suspension was further aged under continuous stirring for 2 hours to complete the precipitation process. The obtained precipitates were thoroughly washed with warm demineralized water until neutral pH (~7), followed by ethanol rinsing, and dried overnight at 70 °C. The resulting citrate-functionalized hydroxyapatite samples were denoted as $(HAp)_5(Cit)_x$ (x = 1, 2, and 4).

2.3 Preparation of HAp nanoparticles

The same protocol was used as described in paragraph 2.2 without using citric acid.

2.4 In situ synthesis of $Au/(HAp)_5(Cit)_x$ catalysts (x= 1; 2; 3 and 4)

Citrate-functionalized hydroxyapatite materials, $Au/(HAp)_5(Cit)_x$, were employed as supports for the in-situ deposition of gold nanoparticles through a one-pot synthesis strategy The presence of surface citrate species was expected to provide coordination sites for gold precursors and promote the formation of supported Au nanoparticles. Typically, 250 mg of $Au/(HAp)_5(Cit)_x$ support (x = 1, 2 and 4) was dispersed in 2 mL of aqueous sodium tetra-chloro-aurate (III) solution ($NaAuCl_4$, 2.5 mmol L^{-1}), corresponding to a theoretical gold loading of 0.4 wt%. The suspension was stirred under reflux at 100 °C for 5 hours. During the process, the initial yellow coloration of the gold precursor solution gradually turned purple, suggesting the in-situ reduction of Au species and the formation of gold nanoparticles. After cooling to room temperature, the solid phase was recovered by centrifugation, washed twice with deionized water and subsequently with ethanol, then dried overnight at 70°C. The resulting catalysts were denoted as $Au/(HAp)_5(Cit)_x$ (x = 1, 2 and 4).

2.5. Preparation of citrate-free Au/HAp catalyst as reference

A citrate-free Au/HAp catalyst was prepared as a reference material using a conventional impregnation–reduction approach. Typically, 250 mg of pristine hydroxyapatite was dispersed in an aqueous solution of sodium tetra-chloro-aurate (III) ($NaAuCl_4$, 2.5 mmol L^{-1}) under continuous stirring. The suspension was heated at 100 °C under atmospheric pressure until complete evaporation of the solvent, allowing the deposition of gold precursor species onto the HAp surface. The resulting solid was subsequently treated with an aqueous sodium borohydride solution ($NaBH_4$, 0.1 mol L^{-1}) to reduce the adsorbed gold species into metallic gold nanoparticles. The catalyst was recovered by centrifugation, washed twice with deionized water

and finally with ethanol, followed by drying at 70 °C overnight. The obtained material was denoted as Au/HAp.

2.6 Characterization methods

The X-ray diffraction (XRD) patterns of all samples were determined using a PANalytical X'Pert PRO powder diffractometer equipped with a fast X'Celerator detector with monochromatic Cu Kα source (λ = 0.15418 nm) using a source power of 40 kV and 40 mA. The samples were characterized using a Bruker Optics Vertex 80 V FT-IR spectrometer in the range of 4000-400 cm^{-1}. Chemical analyses were performed by ICP-OES on a Horiba Jobin Yvon modele activa. The specific surface areas (S_{BET}) were calculated according to the Brunauer-Emmet-Teller (BET) method using a Micromeritics TriStar instrument, based on the N_2 adsorption-desorption data obtained at 77K. The XPS measurements were carried out using a MAC2 type spectrometer whose source is a double aluminum and magnesium anode. The primary beam used is aluminum, with energy hν = 1486.6 eV. The analyzer is geometry cylindrical and its energy resolution is 1eV. The morphology of the catalysts prepared was determined by transmission electron microscopy (TEM-HR) using a JEOL 2010 device operating at 200kV equipped with EDX capacitors. The catalyst powders were dispersed onto carbon-coated copper grids prior to TEM analysis. Carbon amount is measured using a Horiba Jobin Yvon CHNS elemental analyzer, model EMIA 220.

2.6. Free solvent catalytic test

The catalytic oxidation of benzyl alcohol (BzOH) was carried out under solvent-free conditions in a stirred batch autoclave. In a typical experiment, benzyl alcohol (10 mmol, ~1 mL) was introduced into the reactor and purged with nitrogen to remove dissolved oxygen. Subsequently, 25 mg of Au-based catalyst was added, and the reactor was pressurized with molecular oxygen (5 bars) after reaching the desired reaction temperature. The oxidation reaction was conducted at 80 °C under continuous stirring (500 rpm) for 90 min. During the reaction, aliquots were withdrawn every 15 min, diluted with isopropanol containing chlorobenzene (2 wt%) as an external standard, and analyzed by gas chromatography (Varian CP-8450 GC) equipped with a 30 m Carbowax capillary column. The catalytic stability of the hybrid catalysts was evaluated by comparing their performance after synthesis and after 12 months of storage under ambient conditions. Catalyst recyclability was assessed through consecutive catalytic cycles. After each run, the catalyst was recovered by solvent evaporation, dried under vacuum at 150°C for 10 min, and directly reused under identical reaction conditions.

The benzyl alcohol conversion, product selectivity, yield, and turnover frequency (TOF) were calculated according to the following equations:

$$Conversion\ (\%) = \frac{([BzOH]i - [BzOH]t)}{[BzOH]i} \times 100 \quad \textbf{(1)}$$

$$Selectivity\ (\%) = \frac{[Product]i}{\sum[Product]} \times 100 \quad \textbf{(2)}$$

$$Yield\ (\%) = Conversion \times selectivity \quad \textbf{(3)}$$

$$TOF = \frac{number\ of\ mol\ of\ BzOH\ converted}{number\ of\ mol\ of\ gold \times time} \quad \textbf{(4)}$$

2.7. Green Chemistry and Sustainability

The E-factor **(Eq.5)** quantifies the amount of waste generated per unit mass of product and serves as a key indicator in promoting waste minimization and resource efficiency [25, 26]. It has played a central role in the development of cleaner, waste-free chemical processes. As a practical metric of a reaction's greenness, lower E-factor values (approaching zero) reflect processes that are more sustainable and environmentally benign:

$$E - factor = \frac{mass\ of\ waste}{mass\ of\ desired\ product} \quad \textbf{(5)}$$

Mass productivity (MP) **(Eq.6)** accounts for all materials involved in the reaction, including reagents, solvents, catalysts, and any other components. It represents the percentage ratio of the mass of the desired product to the total mass of all inputs. MP is defined as the reciprocal of the mass intensity (MI), expressed as a percentage **(Eq. 6)**. Moreover, mass intensity and the E-factor are intrinsically related, as described by **Eq.6-7** The carbon efficiently (CE) was determined using **Eq.8**.

$$MP(\%) = \frac{mass\ of\ desired\ product}{mass\ of\ all\ used\ reagent} \times 100 = \frac{1}{MI} \times 100 \quad \textbf{(6)}$$

$$E - factor = MI - 1 \quad \textbf{(7)}$$

$$CE = \frac{Number\ of\ carbon\ atoms\ (product)}{Number\ of\ carbon\ atoms\ (reagents)} \quad \textbf{(8)}$$

3. Results and discussion

3.1. Au/$(HAp)_5(Cit)_x$ physico-chemical properties

The crystallin form of the Au/HAp and Au/$(HAp)_5(Cit)_x$ is determined by the XRD analysis (**Fig. 1**).

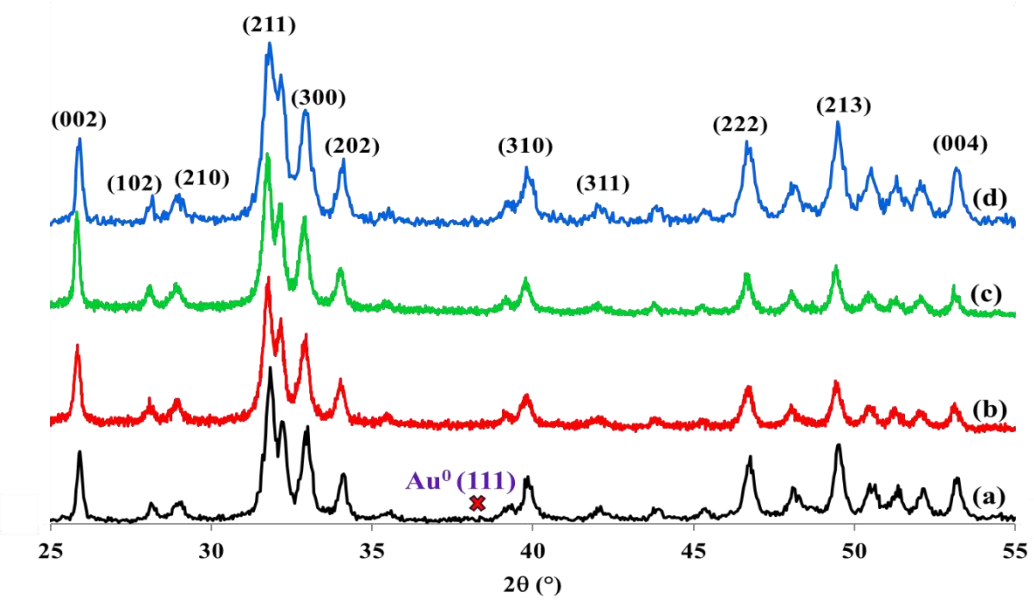


Fig. 1: XRD diffractograms for different catalyst: (a) Au/HAp; (b) Au/$(HAp)_5(Cit)_1$; (c) Au/$(HAp)_5(Cit)_2$; (d) Au/$(HAp)_5(Cit)_4$

The structural integrity of hydroxyapatite after citrate functionalization and gold deposition was first investigated by X-ray diffraction (XRD). As shown in **Fig. 1,** all catalysts exhibit the characteristic diffraction pattern of hexagonal hydroxyapatite (JCPDS No. 09-0432), with reflections located at 2θ = 25.95°, 31.77°, 32.86°, 39.90°, 46.69°, 49.58°, and 53.31°, corresponding to the (002), (211), (300), (310), (222), (213), and (004) crystallographic planes, respectively. The preservation of these diffraction features after citrate modification and Au deposition confirms that the HAp framework remains stable during the functionalization and metal incorporation processes. Interestingly, no diffraction peaks associated with crystalline Au^0 are detected for citrate-containing catalysts, suggesting the formation of highly dispersed gold species or metallic nanoparticles with dimensions below the XRD detection limit. In contrast, the citrate-free Au/HAp catalyst exhibits an additional reflection at 2θ ≈ 38.2°, assigned to the (1 1 1) plane of face-centred cubic metallic gold (JCPDS No. 04-0784), indicating the presence of larger Au crystallites. This distinct structural behaviour highlights the crucial role of citrate molecules in regulating gold nucleation and growth on the HAp surface *[27]*. The enhanced dispersion of Au species in citrate-functionalized catalysts can be attributed to the formation of citrate-mediated interfacial coordination environments. The carboxylate groups of citrate molecules can interact strongly with surface Ca^{2+} sites of HAp, generating anchoring sites that favor the homogeneous deposition of gold precursors and limit their surface migration during nanoparticle formation. In the absence of citrate, the weaker interaction between Au species and pristine HAp likely promotes nanoparticle migration and

coalescence, leading to the formation of larger crystalline Au domains. These observations demonstrate that citrate modification provides an effective molecular-level strategy for controlling the dispersion state of supported gold species through the engineering of the Au–HAp interface.

The chemical nature of citrate incorporation and its influence on the HAp surface was investigated by ATR-FTIR spectroscopy (**Fig. 2**). The spectrum of citric acid displays the characteristic vibrational bands associated with carboxylic functionalities, including the C=O stretching vibration at 1725 cm^{-1} and the asymmetric and symmetric stretching modes of carboxylate groups at 1585 and 1391 cm^{-1}, respectively [28, 29]**(Fig. S2).** After citrate functionalization of HAp, the disappearance of the carbonyl vibration at 1725 cm^{-1} together with the shift of the carboxylate bands toward lower wavenumbers (from 1585 to 1577 cm^{-1} and from 1391 to 1343 cm-1) indicates a strong interaction between citrate molecules and the HAp surface. These spectral modifications suggest the deprotonation of citrate carboxylic groups followed by coordination with exposed Ca^{2+} surface sites, leading to the formation of citrate–calcium interfacial complexes. Furthermore, the appearance of additional bands at 2989 and 2900 cm^{-1}, assigned to C–H stretching vibrations of citrate organic moieties, confirms the successful incorporation of citrate species onto the HAp surface. The broad absorption band centered at approximately 3375 cm^{-1} corresponds to O–H stretching vibrations arising from hydroxyl groups and adsorbed water molecules, reflecting hydrogen-bonding interactions within the modified surface environment.

Following Au deposition, the characteristic citrate-related vibration at 1343 cm^{-1} and the O–H stretching band become less pronounced, suggesting that the local vibrational environment of surface citrate species is modified upon interaction with gold species. These changes may originate from citrate-mediated stabilization of deposited Au nanoparticles, where citrate molecules act as interfacial ligands between the inorganic support and metallic phase. Importantly, the absence of new vibrational features indicates that citrate remains chemically preserved during gold incorporation, maintaining the functionalized HAp surface architecture.

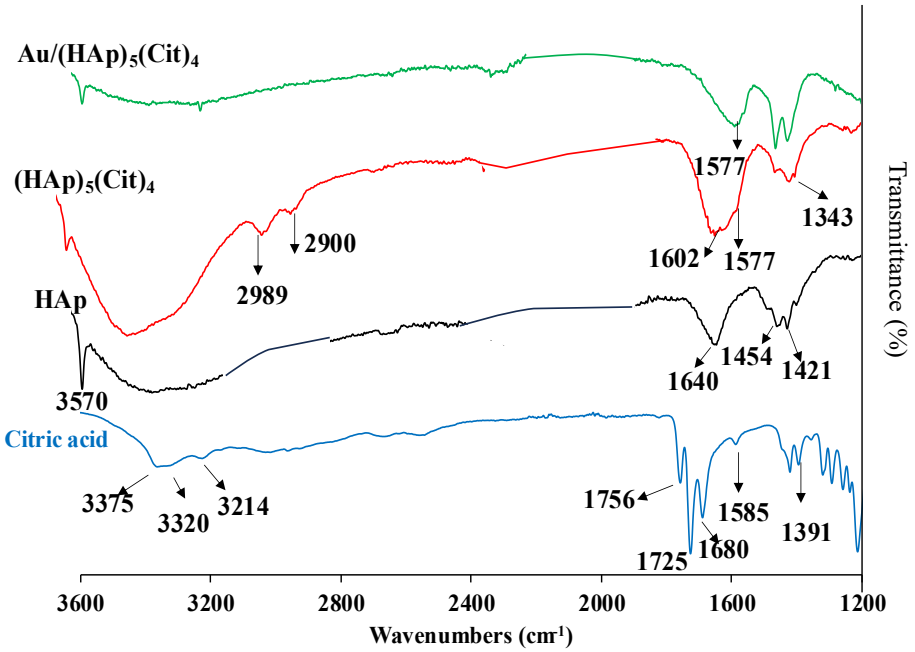


Fig. 2: IR-ATR spectra of Citric acid, HAp, $(HAp)_5(Cit)_4$ and $Au/(HAp)_5(Cit)_4$

The textural properties of $Au/(HAp)_5(Cit)_x$ catalysts were investigated by N_2 adsorption–desorption measurements (**Fig. 3**). All catalysts exhibit type IV isotherms accompanied by hysteresis loops in the relative pressure range of 0.4–0.9, characteristic of mesoporous materials according to the IUPAC classification. The presence of mesoporosity is beneficial for catalytic applications as it facilitates reactant diffusion and provides accessible surface sites for metal–support interactions.

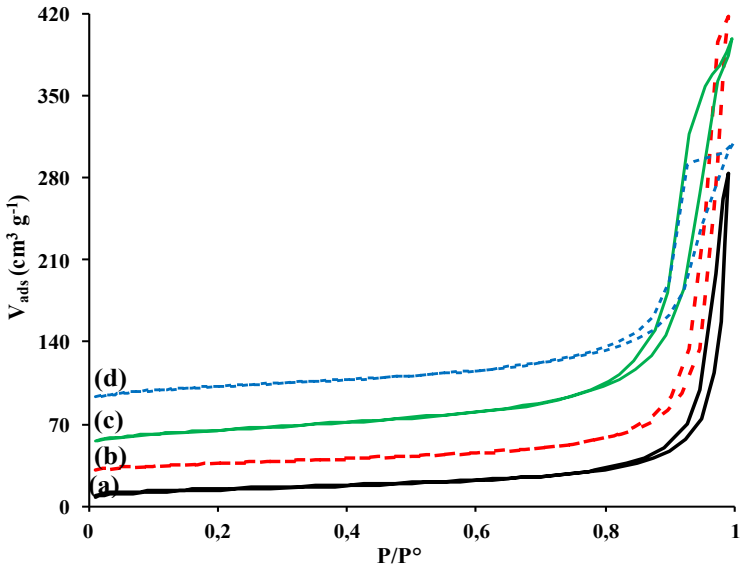


Fig. 3: N_2-adsorption-desorption isotherms for $Au/(HAp)_5(Cit)_x$ catalysis: (a) x=0; (b) x=1, (c) x=2; (d) x=4

The corresponding textural parameters, including specific surface area (S_{BET}), pore volume, average pore diameter, surface basicity (pH_{PZC}), gold loading, and Ca/P ratio, are summarized in Table 1. A progressive increase in surface area is observed with increasing citrate content, from 62 m^2 g^{-1} for Au/HAp to 144 m^2 g^{-1} for Au/$(HAp)_5(Cit)_4$. This enhancement is accompanied by an increase in pore volume (0.36–0.59 cm^3 g^{-1}) and a decrease in average pore diameter (22.8–17.3 nm), suggesting that citrate modification influences the surface organization and porosity of HAp.

The increase in surface area after citrate incorporation can be associated with the interaction of citrate molecules with surface calcium sites, which may prevent particle aggregation during synthesis and generate a more open surface structure. Moreover, the progressive decrease in pHPZC from 8.0 for pristine Au/HAp to 6.5 for Au/$(HAp)_5(Cit)_4$ confirms the modification of the surface acid–base properties by citrate functionalization. This evolution reflects the introduction of acidic carboxylate functionalities and the modification of the local surface charge environment, which may influence both gold anchoring and reactant adsorption during catalytic oxidation [30]. Also, the Ca/P molar ratio increases with citrate content, indicating a modification of the surface calcium environment rather than a structural transformation of the HAp phase. This supports the formation of citrate–Ca^{2+} interactions, consistent with FT-IR observations, and highlights the role of citrate as a surface engineering agent capable of simultaneously tuning the physicochemical properties of HAp and the dispersion of supported gold species.

Table 1: Gold loading (ICP-AES) and textural properties of different catalysts Au/$(HAp)_5(Cit)_x$ (x=0; 1; 2 and 4)

Support $(HAp)_5(Cit)_x$	S_{BET} (m^2 g^{-1})	V_p (g cm^{-3})	D_p (nm)	pH_{PCN}*	Au %	Ca/P ratio
x=0	62 (59) *	0.36	22.8	8.0	0.392	1.668(1.671) *
x =1	74 (88) *	0.41	24.3	7.6	0.226	1.681(1.672) *
x =2	97(118) *	0.48	19.8	7.0	0.364	1.826(1.828) *
x =4	144(182) *	0.59	17.3	6.5	0.393	1.838(1.833) *

()*: value of support

The electronic structure of Au/$(HAp)_5(Cit)_x$ catalysts was investigated by X-ray photoelectron spectroscopy (**Fig. 4**). All samples exhibit similar survey spectra, confirming that citrate functionalization preserves the chemical composition of the hydroxyapatite support while modifying the local surface environment. The O 1s spectra can be deconvoluted into two main contributions centered at approximately 531.1 eV and 532.6 eV, assigned to oxygen atoms

belonging to carboxylate/carbonyl species (C=O/COO^-) and C–O functionalities together with surface hydroxyl groups and adsorbed oxygen species of hydroxyapatite, respectively [31, 32]. The persistence of these contributions after gold deposition indicates that citrate remains anchored to the HAp surface and continues to participate in the interfacial environment surrounding the supported Au nanoparticles. The Au 4f spectra display the characteristic spin–orbit doublet of metallic gold, with Au $4f_{7/2}$ and Au $4f_{5/2}$ components located at approximately 83.3 eV and 87.2 eV, confirming that gold is predominantly present as Au^0 [33–35]. No detectable contribution associated with oxidized Au species is observed, suggesting an efficient reduction of the Au precursor during catalyst preparation. A noticeable positive shift of the Au 4f binding energies is observed for $Au/(HAp)_5(Cit)_4$ relative to the citrate-free Au/HAp catalyst, amounting to approximately 0.70 eV for Au $4f_{7/2}$ and 0.60 eV for Au $4f_{5/2}$. Such shifts indicate that citrate functionalization modifies the electronic environment of supported Au nanoparticles. Rather than reflecting a change in gold oxidation state, these variations are more likely associated with interfacial charge redistribution arising from strong interactions between Au nanoparticles and the citrate-functionalized HAp surface. The coordination of citrate carboxylate groups with surface Ca^{2+} sites is expected to modify the local electrostatic environment surrounding Au nanoparticles, thereby influencing the electron density of surface Au atoms. Similar electronic perturbations have been reported for ligand-modified supported noble-metal catalysts and are frequently associated with changes in reactant adsorption strength and oxygen activation. Surface elemental compositions further support this interpretation (**Table 2**). Whereas the P and O contents remain nearly constant throughout the catalyst series, confirming preservation of the HAp framework, the progressive increase in surface carbon concentration demonstrates the successful incorporation of citrate species. Simultaneously, the Au/Ca atomic ratio increases with citrate loading, indicating a greater surface concentration of accessible Au species. This trend suggests that citrate functionalization promotes a more efficient immobilization of Au precursors, most likely through the creation of additional coordination sites capable of stabilizing gold during nucleation. Collectively, the XPS results demonstrate that citrate acts not only as a stabilizing ligand but also as an interfacial electronic modifier capable of regulating both the dispersion and electronic properties of supported Au nanoparticles [36, 37].

Table 2: XPS results for different catalysts

$Au/(HAp)_5(Cit)_x$	$\%Au^0$	Au/Ca	%P	%O	%C
x=0	0.289	0.013	8.59	69.15	0.80
x =1	0.180	0.008	8.78	68.61	2.10
x =2	0.323	0.017	8.63	69.96	3.31
x =4	0.482	0.020	8.20	69.81	4.79

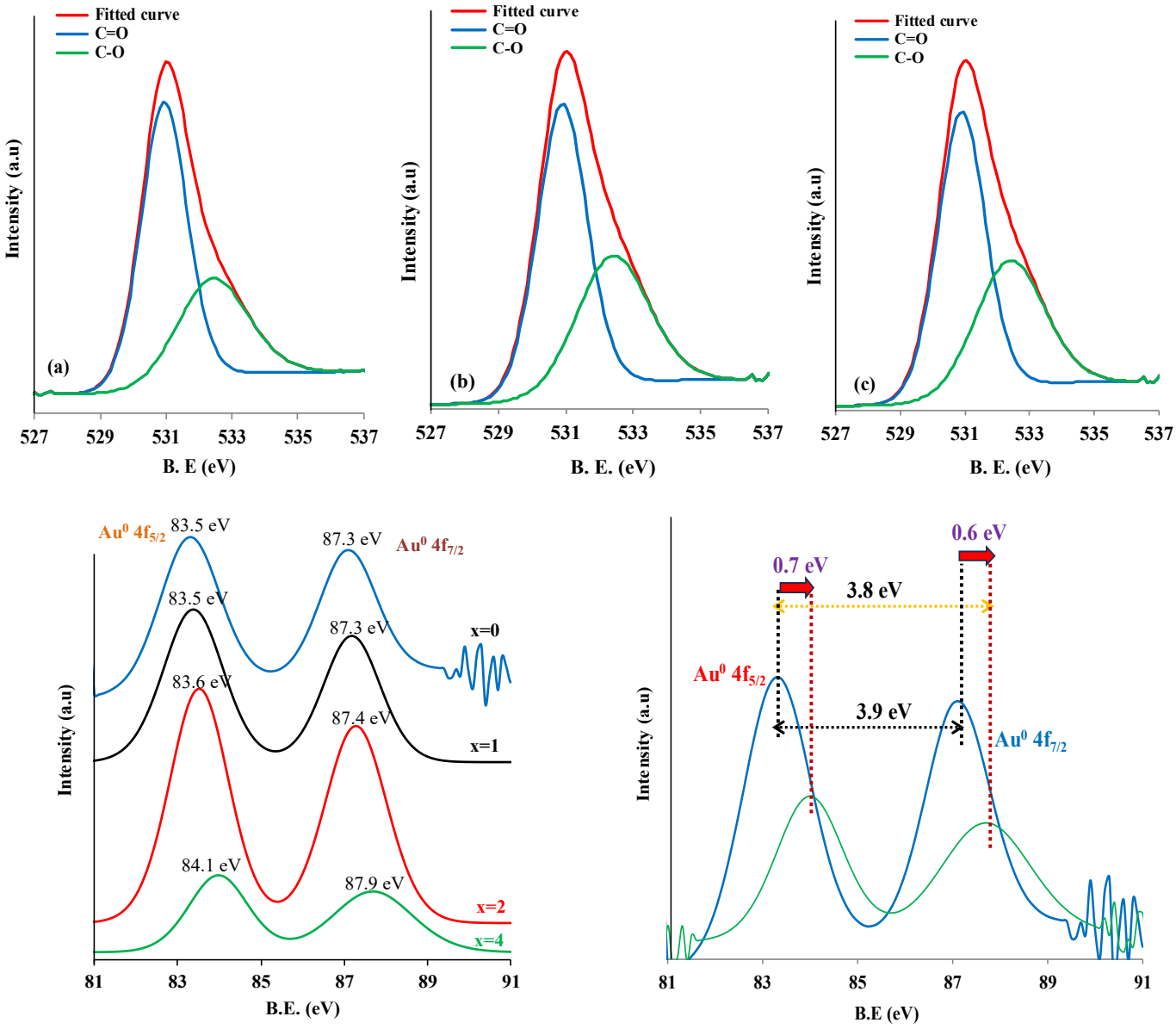


Fig. 4:XPS spectra of different $Au/(HAp)_5(Cit)_x$ catalysis: A: (a): x=; (b) x=2; (c): x=4 and B: (a): XPS spectra and (b) comparative XPS between Au/HAp and $Au/(HAp)_5(Cit)_4$

3.2. Morphological properties

The influence of citrate functionalization on catalyst morphology was investigated by SEM, EDX and high-resolution TEM analyses. SEM images (**Figs S4 and S5**) reveal significant differences between the citrate-free Au/HAp catalyst and citrate-functionalized samples. The pristine catalyst is characterized by irregular aggregates with extensive particle coalescence, whereas citrate-containing materials display a more homogeneous morphology together with a marked reduction in aggregation. Elemental analysis confirms the homogeneous distribution of Ca, P and O from the hydroxyapatite matrix together with Au throughout the catalyst particles, demonstrating successful incorporation of the metallic phase. The comparable overall Au signal intensity among the different catalysts indicates that citrate primarily affects the spatial distribution of gold rather than its global loading. High-resolution TEM provides direct evidence for the effect of citrate on Au nanoparticle formation (**Fig. 5**). In citrate-functionalized catalysts, Au nanoparticles are uniformly dispersed over the HAp surface and exhibit a narrow size distribution. In contrast, the citrate-free catalyst contains larger particles together with a broader particle size distribution, in agreement with the XRD observations showing detectable crystalline Au domains.

The improved dispersion observed after citrate functionalization can be rationalized by considering the role of citrate during Au nucleation. Surface-bound citrate molecules coordinated to Ca^{2+} sites generate a high density of anchoring centers that facilitate homogeneous adsorption of Au precursor species. Consequently, nucleation is expected to occur simultaneously at numerous surface sites, leading to the formation of a larger number of nuclei while suppressing particle migration and coalescence during reduction. In the absence of citrate, the lower density of anchoring sites allows greater mobility of Au species, favoring Ostwald ripening and particle growth [38]. A schematic representation of this proposed mechanism is presented in **Fig. 6.** In contrast, the citrate-free Au/HAp catalyst exhibits weaker interactions between gold species and the support surface, leading to less controlled nucleation, larger particle domains, and a broader particle size distribution. These results demonstrate that citrate functionalization provides an effective strategy for tuning Au nanoparticle growth through interfacial regulation. The resulting control over nanoparticle size and dispersion is expected to enhance the availability of surface-accessible active sites and thereby influence the catalytic behavior of Au/HAp-based catalysts.

The combined XRD, XPS and TEM results therefore establish a clear structure–property relationship in which citrate-mediated surface engineering controls both the nucleation kinetics and the electronic environment of supported Au nanoparticles. Such simultaneous regulation of

particle dispersion and metal–support interactions is expected to directly influence oxygen activation and the catalytic oxidation of benzyl alcohol, as discussed in the following section.

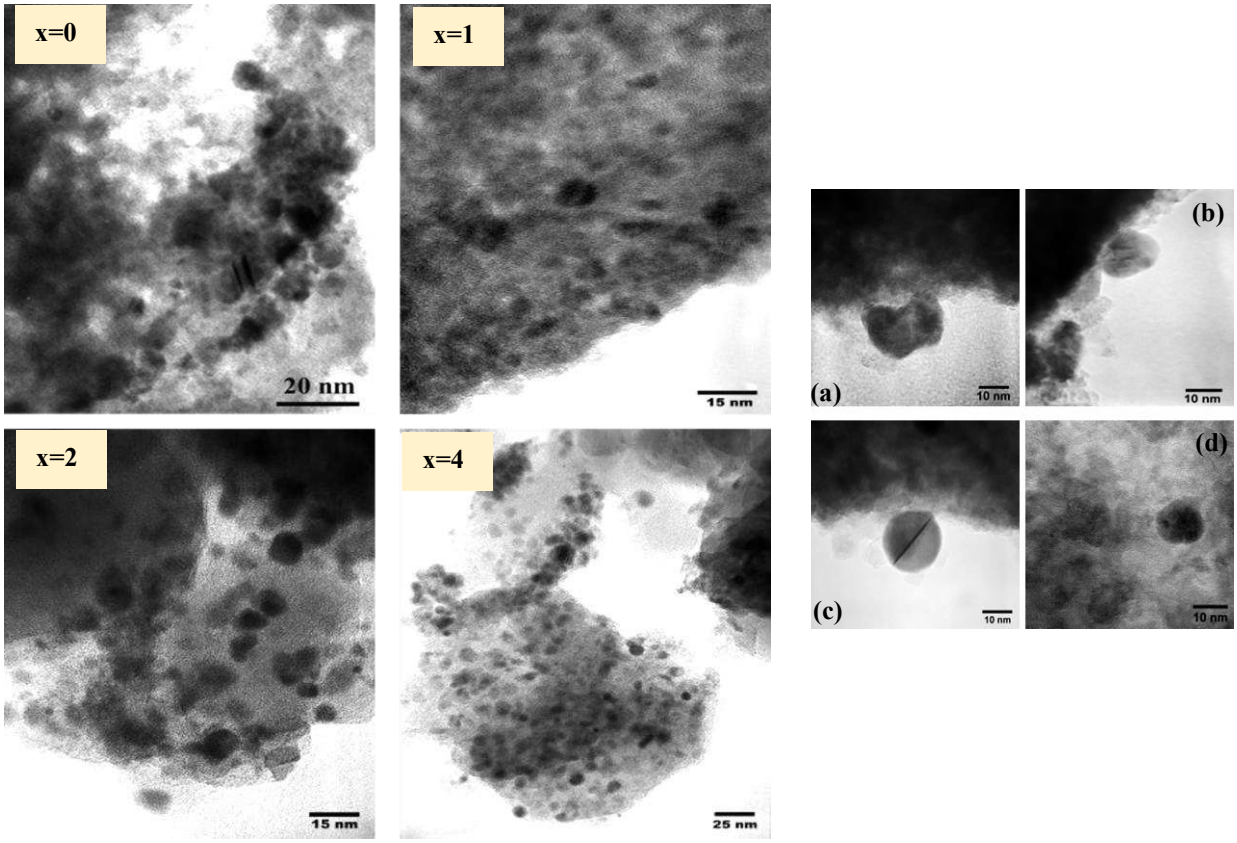


Fig. 5: TEM micrographs of Au/(HAp)$_5$(Cit)$_x$: (a) x=0; (b) x=1; (c) x=2 and (d)x=4

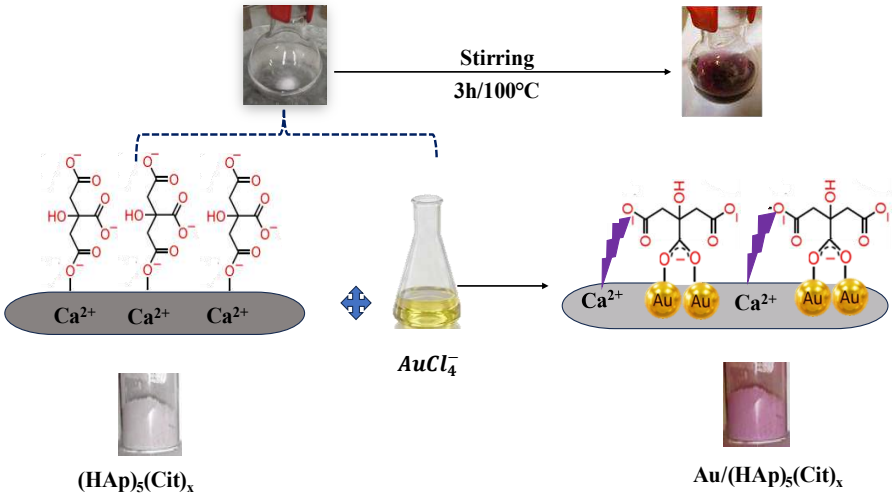


Fig. 6: Proposed mechanism of gold nanoparticles reduction

4. Solvent free Benzyl alcohol oxidation

4.1.Effect of HAp/Cit molar ratio

The catalytic activity of the Au/$(HAp)_5(Cit)_x$ materials was investigated in the aerobic oxidation of benzyl alcohol to assess the effect of citrate functionalization on catalyst performance. Time–conversion plots were recorded and are presented in **Fig. 7**.

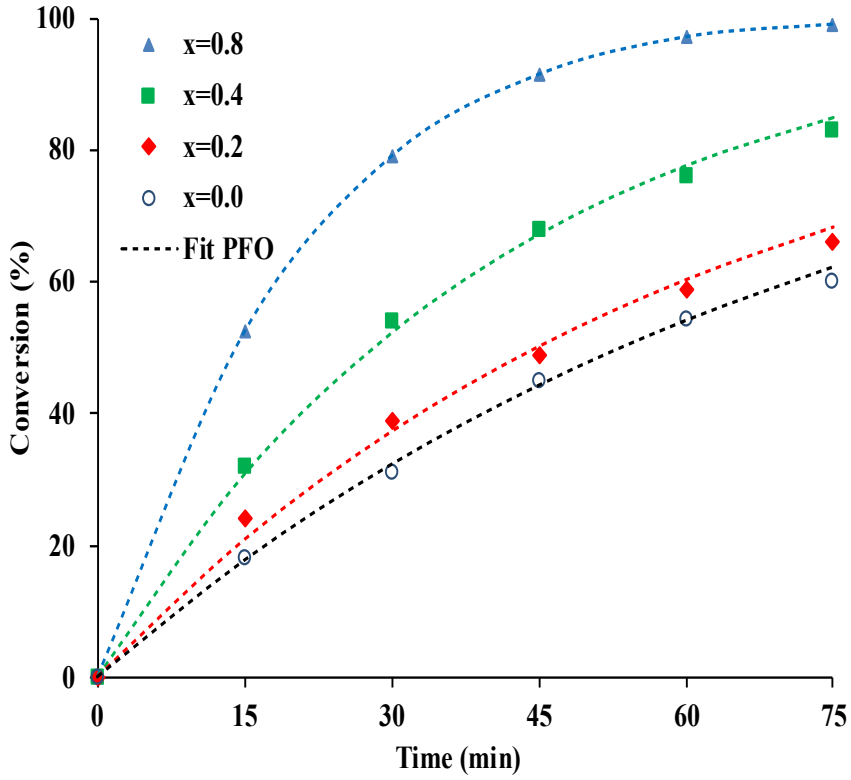


Fig. 7: Oxidation of benzyl alcohol by various gold catalysts

Reaction conditions: *benzyl alcohol:10 mmol, gold catalyst: 25 mg, T=80°C, t=75 min,* P_{O2} *= 5 bars*

The kinetics of benzyl alcohol oxidation reveal a pronounced dependence of catalytic activity on the degree of citrate functionalization of the hydroxyapatite support. All catalysts exhibit a monotonic increase in conversion with reaction time under conditions of excess molecular oxygen. More importantly, citrate incorporation systematically enhances the catalytic performance, although the activity does not scale linearly with citrate loading, indicating a complex interplay between nanoparticle stabilization, surface accessibility, and metal–support interactions.

4.2.Kinetic evaluation of Au/$(HAp)_5(Cit)_x$ catalysts in the aerobic oxidation of Benzyl Alcohol

Kinetic evaluation of Au/$(HAp)_5(Cit)_x$ catalysts in the aerobic oxidation of benzyl alcohol revealed that the reaction follows a first-order dependence on substrate concentration **(Fig. S6)**. In the present study, the rate expression for this system can be formulated as:

$$\boldsymbol{v = k \times P_{O2}^{\alpha} \times [BzOH]^{\beta}} \quad \textbf{(9)}$$

where v is the rate of benzyl alcohol, k the rate constant, P_{O2} the pressure of oxygen, [BzOH] the concentration of benzyl alcohol, a and b the partial orders in O_2 and BzOH respectively. The O_2 pressure is in excess; the **Eq.10** can be simplified by **Eq.11**:

$$\boldsymbol{v = k \times P_{O2}^{\alpha} \times [BzOH]^{\beta} = k_{app} \times [BzOH]^{\beta}} \qquad \textbf{(10)}$$

The kinetic data were linear fitted using a pseudo-first-order model:

$$\boldsymbol{ln\frac{[BzOH]_t}{[BzOH]_i} = -k_{app} \times t} \qquad \textbf{(11)}$$

where $[BzOH]_t$ is the benzyl alcohol concentration (mol L^{-1}) at time t, $[BzOH]_i$ is benzyl alcohol concentration (mol L^{-1}) at initial time (t=0), and k_{app} is the apparent rate constant (min^{-1}). The fitting results, the corresponding conversion values and turnover frequencies (TOF) are summarized in **Table 3**. Statistical error functions such as MSE, RSME and RMPD (%) in the pseudo-first order kinetic modeling of benzyl alcohol oxidation were determined using the equations:

$$MSE = \frac{1}{N}\sum_{i=1}^{N}(experimental - calculated)^2 \qquad \textbf{(12)}$$

$$RMSE = \sqrt{\frac{1}{N}\sum_{i=1}^{N}(experimental - calculated)^2} \qquad \textbf{(13)}$$

$$MRPD = \frac{100}{N}\sum_{i=1}^{n}\left|\frac{experimental - calculated}{experimental}\right| \qquad \textbf{(14)}$$

The catalytic performance of Au/$(HAp)_5(Cit)_x$ catalysts was evaluated in the solvent-free aerobic oxidation of benzyl alcohol under mild reaction conditions (Fig. 7). The citrate-free Au/HAp catalyst exhibited a benzyl alcohol conversion of 60% with a turnover frequency (TOF) of 149.68 h^{-1}, in agreement with the activity generally reported for supported Au catalysts under comparable aerobic oxidation conditions [39]. Progressive citrate functionalization markedly improved the catalytic performance, demonstrating that surface engineering of the HAp support strongly influences the reactivity of supported Au nanoparticles.

Introducing a low citrate loading (x = 1) increased the conversion to 66%, while the TOF rose sharply to 250.74 h^{-1}. This significant enhancement cannot be solely attributed to the amount of deposited gold, which remains nearly constant, but is more likely associated with the improved dispersion of Au nanoparticles evidenced by XRD and TEM together with the modified interfacial electronic environment revealed by XPS. The coordination of citrate molecules to surface Ca^{2+} sites is expected to generate a larger number of homogeneous nucleation centers, leading to a higher density of accessible Au nanoparticles and a stronger metal–support interaction. Further increasing the citrate content to x = 2 resulted in a conversion

of 84%, whereas the TOF slightly decreased to 229.68 h^{-1}. Although the higher conversion reflects the larger population of catalytically accessible Au nanoparticles, the small decrease in intrinsic activity suggests that increasing citrate coverage may progressively modify the local environment of surface Au atoms. Such behavior is consistent with ligand-modified supported catalysts, where surface organic species simultaneously stabilize metallic nanoparticles and partially influence the adsorption strength of reactants or reaction intermediates. Nevertheless, the overall catalytic performance remains superior to that of the citrate-free catalyst, indicating that the beneficial effect of improved Au dispersion outweighs any slight decrease in intrinsic site activity. The $Au/(HAp)_5(Cit)_4$ catalyst exhibited the highest catalytic performance, reaching 99% benzyl alcohol conversion together with a TOF of 401.05 h^{-1}. This remarkable improvement correlates well with the physicochemical characteristics established by XRD, BET, XPS and TEM analyses, including the absence of detectable crystalline Au domains, the highest specific surface area, the largest Au/Ca surface ratio, and the homogeneous dispersion of small Au nanoparticles. These results demonstrate that citrate functionalization simultaneously regulates the nucleation, stabilization and electronic environment of supported Au nanoparticles, generating an optimized Au–HAp interface for catalytic oxidation. Overall, the catalytic results establish a clear structure–activity relationship in which citrate acts as an interfacial engineering agent rather than a simple stabilizing ligand. By coordinating surface Ca^{2+} sites, citrate modifies the surface chemistry of hydroxyapatite, promotes homogeneous Au nucleation, suppresses nanoparticle coalescence and enhances the exposure of catalytically accessible Au sites. The superior activity of $Au/(HAp)_5(Cit)_4$ therefore originates from the synergistic contribution of improved nanoparticle dispersion, optimized metal–support interactions and the tailored surface environment created by citrate functionalization [40].

Table 3: Kinetic analysis and Catalytic properties of Au/(HAp)5(Cit)x catalysis

$Au/(HAp)_5(Cit)_x$	x=0	x=1	x=2	x=4
R^2	0.987	0.998	0.998	0.995
$k_{app}\times10^{-3}$ (min^{-1})	12.7	15.3	22.7	57.8
Conversion * (%)	60 ±2	66±3	83±2	99±1
TOF (h^{-1})**	149.68	250.74	229.68	401.05
MSE	10^{-4}	4×10^{-4}	2×10^{-4}	10^{-4}
RMSE	0.01	0.02	0.01	0.01
MRPD (%)	2.23	5.20	2.52	1.46

4.3. Effect of citrate functionalization on benzaldehyde selectivity

The evolution of benzaldehyde selectivity as a function of citrate loading and reaction time is presented in Fig. 8. During the initial stage of the reaction (up to 45 min), all Au/(HAp)5(Cit)x catalysts exhibit high selectivity toward benzaldehyde, indicating that the citrate-modified catalysts efficiently promote the selective oxidation of benzyl alcohol while limiting consecutive oxidation reactions under moderate conversion levels. However, at extended reaction times, a significant decrease in benzaldehyde selectivity is observed for the highly citrate-functionalized catalysts. For x = 2 and 4, the selectivity decreases to 28% and 8%, respectively, after 60 min. This behavior suggests that the enhanced activity associated with citrate functionalization accelerates not only the initial oxidation of benzyl alcohol to benzaldehyde but also the subsequent oxidation of benzaldehyde into benzoic acid when benzaldehyde accumulates in the reaction medium. In contrast, the citrate-free and low-citrate catalysts (x = 0 and 1) maintain high benzaldehyde selectivity (96–97%) throughout the reaction, which can be attributed to their lower intrinsic oxidation rates and reduced availability of highly active sites responsible for consecutive oxidation. These results demonstrate that citrate incorporation modulates both catalytic activity and product distribution, with the optimal catalytic behavior requiring a balance between sufficient interfacial activation of oxygen/substrate molecules and controlled exposure of highly reactive Au sites. Therefore, citrate loading and reaction time represent complementary parameters for tuning benzaldehyde productivity and selectivity. These results indicate an activity–selectivity trade-off: higher conversion is accompanied by increased consecutive oxidation of benzaldehyde to benzoic acid during extended reaction times.

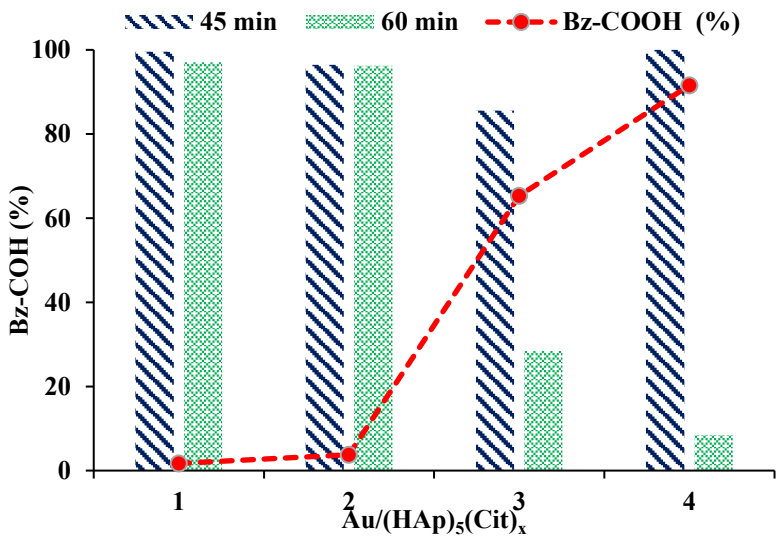


Fig. 8: Effect of time reaction in the Bz-COH selectivity

4.4. Recyclable catalysts $Au/(HAp)_5(Cit)_x$

The recyclability of the **$Au/(HAp)_5(Cit)_x$** catalysts was evaluated over four consecutive oxidation cycles to assess their operational stability under the reaction conditions. While **$Au/(HAp)_5(Cit)_1$** exhibited a slight decline in benzyl alcohol conversion, the **$Au/(HAp)_5(Cit)_2$** and particularly **$Au/(HAp)_5(Cit)_4$** catalysts retained nearly constant catalytic activity, highlighting the beneficial role of citrate functionalization in improving catalyst durability **(Fig. 9)**.

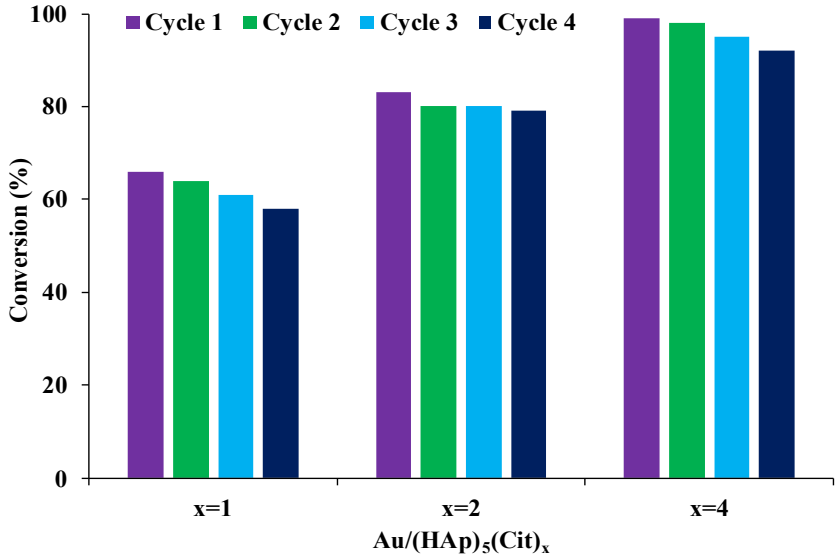


Fig. 9: Conversion stability of the catalysts over recycling cycles

This enhanced stability is attributed to the stronger interfacial interactions established between the citrate carboxylate groups, surface Ca^{2+} sites, and Au nanoparticles, which provide effective anchoring sites that suppress nanoparticle migration and aggregation during catalysis. This interpretation is supported by the XRD, TEM micrographs and N_2 adsorption-desorption of the recycled catalysts **(Fig. 10)**.

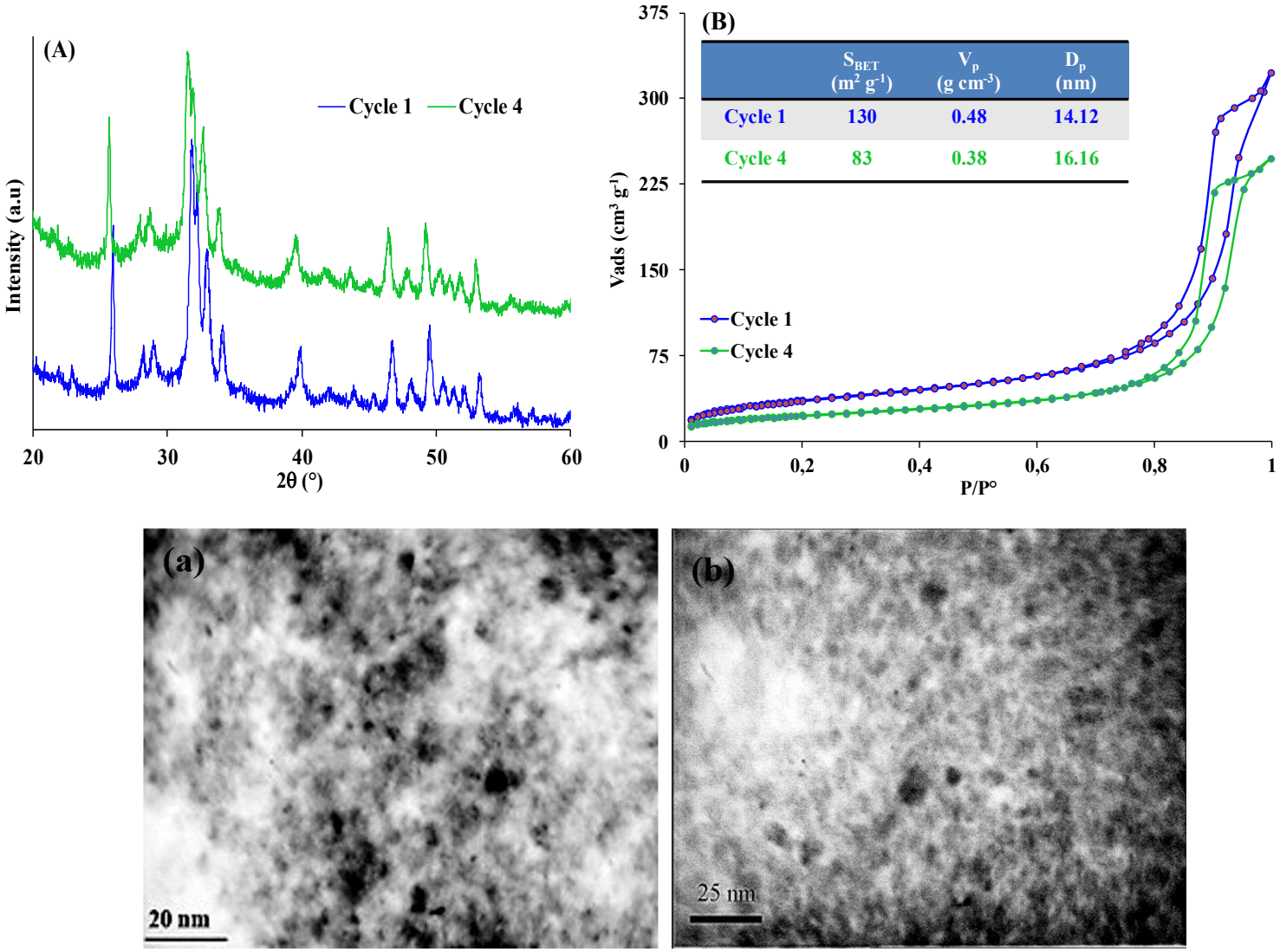


Fig. 10: Effect of Au/$(HAp)_5(Cit)_4$ catalyst recycling on structural, textural and morphological properties: (A) XRD, (B) N_2 adsorption-desorption, (a) TEM after cycle 1 and (b) TEM after cycle 4.

After four catalytic cycles, the BET surface area decreased from 130 to 83 m^2 g^{-1}, accompanied by a reduction in pore volume from 0.48 to 0.38 cm^3 g^{-1} and a slight increase in the average pore diameter. Similar textural changes have frequently been reported for supported noble-metal catalysts after repeated oxidation reactions, where moderate decreases in BET surface area are generally associated with partial pore blockage by strongly adsorbed reaction intermediates or products rather than irreversible collapse of the porous framework [33, 41]. In the present study, this interpretation is supported by the unchanged XRD patterns, which confirm the preservation of the crystalline hydroxyapatite structure and the absence of detectable Au crystal growth. Moreover, post-reaction TEM images show that the Au nanoparticles remain uniformly dispersed over the HAp support without noticeable

aggregation, confirming that the decrease in BET surface area does not originate from nanoparticle sintering but rather from a slight reduction in pore accessibility. Overall, these complementary characterizations demonstrate that the catalyst retains its structural integrity and excellent morphological stability throughout the recycling process.

4.5.Effect of storage time and $NaBH_4$ regeneration treatment

The long-term stability of citrate-functionalized $Au/(HAp)_5(Cit)_x$ catalysts was evaluated by performing benzyl alcohol oxidation after 12 months of storage under ambient conditions (**Table 5**). Compared with the freshly prepared catalysts, all aged materials exhibited a significant decrease in catalytic activity, demonstrating that prolonged storage induces modifications of the active catalytic interface.

Table 4: Catalytic properties for Au/(HAp)5(Cit)x after 12 months

$Au/(HAp)_5(Cit)_x$	Conversion[(a)] (%)	TOF[(b)] (h^{-1})	Au^{0}[(c)] (%)	AuO_x[(c)] (%)
x=1	37 (66) *	217.00	79	21
x=2	53 (84) *	51.94	61	39
x=4	60 (99) *	129.10	65	35

[(a)]*determined after 3 hours;* [(b)] *calculated after 15 min;* [(c)]*determined by XPS* ^{0*} *After regeneration*

The $Au/(HAp)_5(Cit)_4$ catalyst, which exhibited the highest initial activity, showed a decrease in benzyl alcohol conversion from 99 to 60%, accompanied by a decrease in TOF from 401 to 129 h^{-1}. Similar activity losses were observed for catalysts containing lower citrate contents, although the extent of deactivation varied depending on the initial surface environment. These results indicate that the citrate-modified Au/HAp interface, while highly effective for promoting Au dispersion and catalytic activity, remains sensitive to surface evolution during long-term storage. XPS analysis provides important insights into the origin of this deactivation (**Fig. 11 and Fig. S7**). After aging, an increased contribution of oxidized gold species ($Au^{\delta+}$) is observed, reaching up to 39%, together with a decrease in the relative amount of metallic Au^0. This evolution suggests a partial modification of the electronic state of surface gold atoms during storage, likely induced by interactions with surface oxygenated species, hydroxyl groups, or rearrangement of citrate-derived interfacial species [42]. Since metallic Au^0 sites are generally associated with alcohol activation, such electronic modification may reduce the availability of catalytically favorable sites and alter the reaction pathway. In addition to electronic changes,

TEM analysis reveals modifications in the dispersion state and morphology of gold nanoparticles after aging (**Figs S8–S9**). These structural rearrangements may further contribute to the loss of catalytic efficiency by decreasing the number of accessible Au active sites and modifying the metal–support interface. These structural rearrangements may further contribute to the loss of catalytic efficiency by decreasing the number of accessible Au active sites and modifying the metal–support interface. Such deactivation pathways, involving nanoparticle restructuring, loss of dispersion and changes in the electronic state of surface gold species, have been widely reported for supported gold catalysts [43–45]. Moreover, catalyst aging also influences product selectivity. Whereas freshly prepared Au/$(HAp)_5(Cit)_4$ preferentially promotes benzaldehyde formation, aged catalysts exhibit increased benzyl benzoate formation. This change suggests that modification of the Au oxidation state and surface chemical environment affects the relative kinetics of the competing oxidation and coupling pathways. The increased fraction of electron-deficient $Au^{\delta+}$ sites and the modified adsorption environment may favor alternative transformations involving benzyl alcohol/benzaldehyde-derived intermediates, leading to enhanced ester formation [46, 47]. These observations highlight the importance of maintaining an appropriate balance between metallic Au^0 sites and interfacial oxidized species for controlling oxidation selectivity.

To evaluate the reversibility of the observed deactivation, the aged catalysts were subjected to a mild NaBH4 regeneration treatment. Remarkably, the catalytic activity and benzaldehyde selectivity were significantly recovered after reduction, demonstrating that the loss of performance is significantly influenced by reversible surface chemical modifications rather than irreversible structural degradation. The regeneration effect can be attributed to the restoration of metallic Au^0 sites and the removal or transformation of surface oxygenated species that partially block active sites [47–49]. Overall, these results demonstrate that citrate functionalization provides highly active Au/HAp catalysts but that long-term performance depends critically on the preservation of the Au–citrate–HAp interfacial structure. The reversible evolution of Au oxidation state revealed here emphasizes the importance of controlling metal–support interactions and surface electronic properties for designing durable supported gold oxidation catalysts.

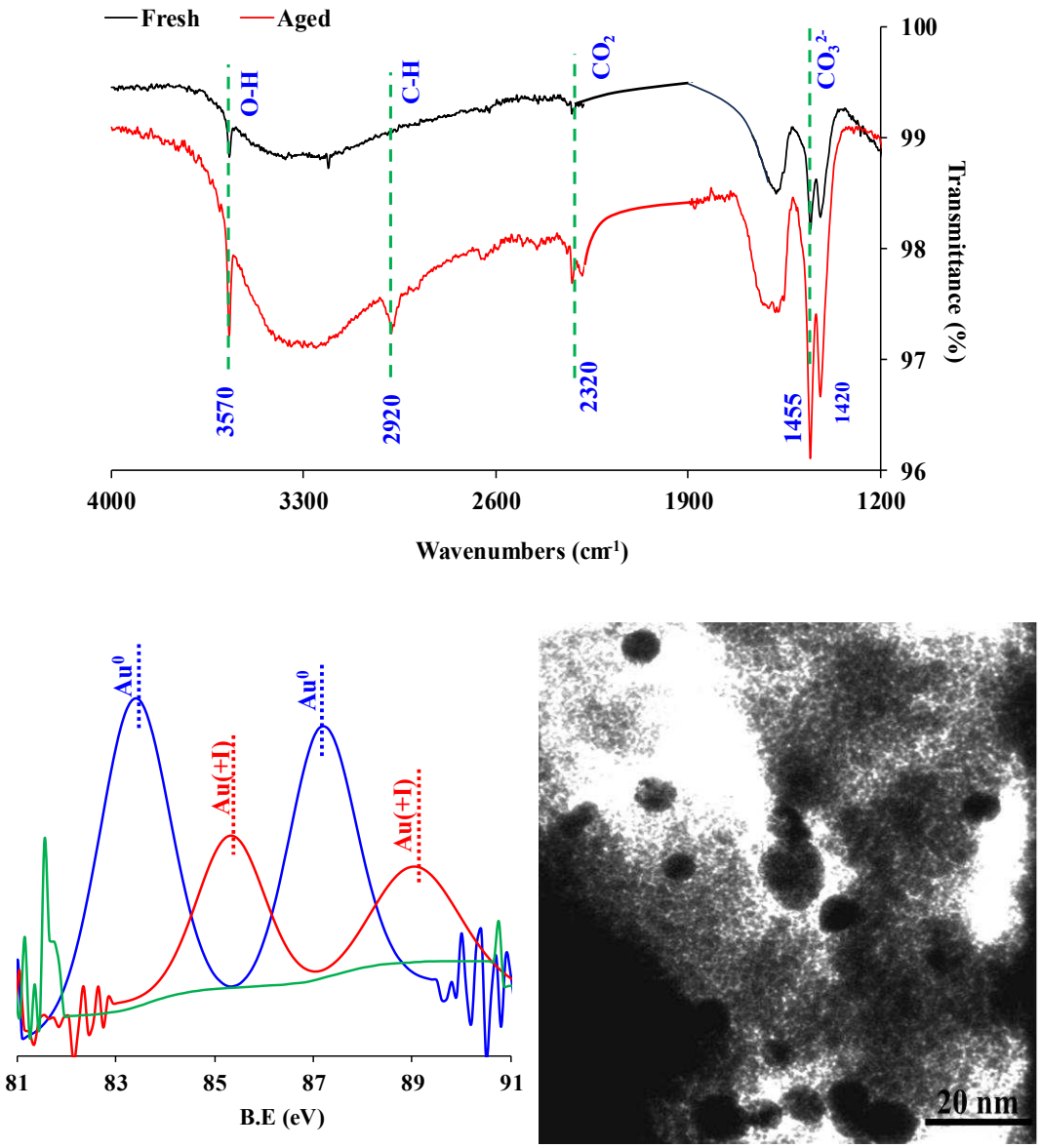


Fig. 11: (A) IR-ATR (B) XPS spectra (C) HR-TEM micrographs for Au/(HAp)$_5$(Cit)$_4$ after 12 months

4.6.Effect of palladium addition (Pd) on Au/(HAp)$_5$(Cit)$_x$ in benzyl alcohol oxidation

The incorporation of Pd into Au/(HAp)$_5$(Cit)$_x$ catalysts markedly modifies both catalytic activity and product selectivity during the solvent-free aerobic oxidation of benzyl alcohol (Table 4). For Au/(HAp)$_5$(Cit)$_1$ and Au/(HAp)$_5$(Cit)$_2$, Pd addition increases the benzyl alcohol conversion from 66 and 83%, respectively, to complete conversion under identical reaction conditions. Such a pronounced enhancement is consistent with the synergistic behavior widely reported for Au–Pd bimetallic catalysts, where the intimate interaction between both metals generates active interfacial sites exhibiting higher catalytic efficiency than the corresponding monometallic counterparts [48, 49]. Although the present characterization does not allow the individual roles of Au and Pd to be unequivocally identified, the improved activity strongly

suggests that Pd modifies the catalytic properties of Au through geometric and electronic effects. The incorporation of Pd may alter the electronic structure of neighboring Au atoms while simultaneously generating new interfacial sites capable of promoting key elementary steps involved in aerobic oxidation. This interpretation is consistent with previous studies showing that Au–Pd alloys or closely contacted Au–Pd nanoparticles facilitate molecular oxygen activation and accelerate catalyst regeneration during alcohol oxidation [50]. Beyond the remarkable increase in activity, Pd incorporation substantially modifies the reaction selectivity. Whereas Au catalysts predominantly produce benzaldehyde, the corresponding Au–Pd catalysts generate comparable amounts of benzaldehyde and benzoic acid, indicating that Pd not only accelerates the oxidation of benzyl alcohol but also promotes the consecutive oxidation of benzaldehyde. This behavior suggests that the overall oxidation pathway is shifted toward deeper oxidation once Pd is introduced into the catalytic interface. The enhanced formation of benzoic acid is likely associated with the higher oxidation capability of Au–Pd interfacial sites together with the favorable adsorption environment provided by the citrate-functionalized HAp support [51]. Under these conditions, the rate of benzaldehyde oxidation becomes comparable to its rate of formation, leading to the simultaneous production of both oxidation products. Such behavior illustrates the kinetic competition between the two consecutive oxidation steps rather than a simple change in catalyst activity [52, 53].

Table 5: Effect of Pd addition in the catalytic performance

		Selectivity (%)		
Pd–Au/$(HAp)_5(Cit)_x$	**Conversion (%)**	**BzOH**	**BzCOOH**	**Time**
x=1	100	46	54	45 min
x=2	100	43	57	60 min
x=4	100	55	45	60 min

4.7. Proposed reaction pathways for benzyl alcohol oxidation over $Au/(HAp)_5(Cit)_x$ catalysts

The aerobic oxidation of benzyl alcohol over supported gold catalysts is generally proposed to proceed through an oxygen-assisted dehydrogenation pathway involving the activation of the alcohol molecule on low-coordinated Au sites. The initial interaction between benzyl alcohol and the gold surface leads to the formation of surface benzyloxy intermediates ($C_6H_5CH_2O^*$), which can undergo further dehydrogenation to produce benzaldehyde. Under conditions where the oxidation of the intermediate is kinetically limited, benzaldehyde remains the predominant product, explaining the high aldehyde selectivity commonly reported for Au-based catalysts under base-free or mildly basic conditions.

The subsequent oxidation of benzaldehyde to benzoic acid occurs through the formation of surface benzoate species generated by the interaction of benzaldehyde-derived intermediates with activated oxygen species. This consecutive oxidation pathway becomes increasingly favorable when oxygen activation is enhanced or when the catalyst surface provides highly reactive oxygen-containing sites. Therefore, controlling the balance between alcohol activation, oxygen availability, and intermediate desorption is essential for achieving high benzaldehyde selectivity. In addition to the aldehyde and acid pathways, benzyl benzoate formation may occur through coupling reactions involving benzyl alcohol-derived benzyloxy species and benzaldehyde intermediates. Such side reactions become more competitive when the surface electronic properties, oxygen activation ability, or intermediate adsorption strength are modified.

For the citrate-functionalized Au/$(HAp)_5(Cit)_x$ catalysts, the catalytic selectivity is therefore expected to depend on the synergistic effects of gold nanoparticle dispersion, Au oxidation state, citrate-mediated interfacial interactions, and the acid–base properties of the hydroxyapatite support. The citrate-modified interface can regulate both the availability of active Au sites and the adsorption strength of oxygenated intermediates, thereby influencing the competition between benzaldehyde formation, further oxidation to benzoic acid, and coupling pathways leading to benzyl benzoate (**Fig. 13**). These considerations highlight the importance of controlling the Au–citrate–HAp interfacial environment to tune catalytic activity and product selectivity.

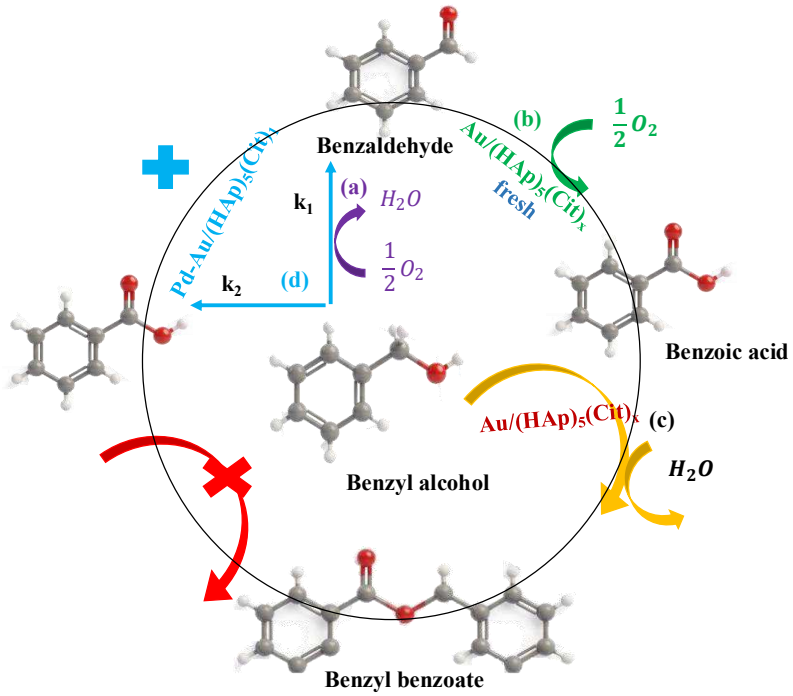


Fig. 12: Proposed mechanism of benzyl alcohol oxidation using fresh and reduced: (a) All catalysts, (b) $Au/(HAp)_5(Cit)_x$ (c) $Au/(HAp)_5(Cit)_x$ aged and (c) Pd_1-$Au_2/(HAp)_5(Cit)_4$

4.8. Green metrics and catalytic efficiency

The catalytic performance of the $Au/(HAp)_5(Cit)_x$ series improves significantly with increasing citrate content **(Table 6)**. Mass productivity (MP) increases progressively from 57% for x = 0 to 95% for x = 4, while the E-factor, which expresses the amount of waste generated relative to the mass of the desired product, decreases sharply from 0.7 to 0.05. This inverse correlation reflects improved overall oxidation process efficiency in the presence of citrate groups. Simultaneously, carbon efficiency (CE) increases from 59% to 99%, indicating near-complete utilization of the carbon substrate and a significant reduction in non-productive side reactions. These results highlight the beneficial role of citrate groups in modulating the physicochemical properties of catalysts. Indeed, citrate acts as a multidentate ligand capable of simultaneously coordinating the Ca^{2+} sites of hydroxyapatite and gold nanoparticles, thus promoting homogeneous metal dispersion and stabilizing active sites. Furthermore, the carboxylate and hydroxyl groups of citrates can facilitate the activation of molecular oxygen and stabilize reaction intermediates, thereby accelerating the catalytic cycle and improving the selectivity of the process [54]. Similar effects have been reported for gold catalysts modified with carboxylate ligands, where the presence of these surface species promotes electron transfer and maintains the redox dynamics of the active sites. Thus, the high performance of the $Au/(HAp)_5(Cit)_4$ catalyst (MP = 95%, E-factor = 0.05, CE = 99%) can be attributed to an optimized electronic and structural environment induced by the presence of citrate, leading to efficient oxidation of the substrate with minimal formation of by-products and excellent atom economy [55–57].

Table 6: Green metrics values of different catalysts of different gold catalysts supported on hydroxyapatite

$Au/(HAp)_5(Cit)_x$	MP (%)	E-factor	CE (%)
x=0	57	0.7	59
x=1	61	0.65	65
x=2	68	0.47	83
x=4	95	0.05	99

5. Conclusion

This work establishes citrate-functionalized hydroxyapatite as an effective support for the controlled synthesis of highly dispersed Au nanoparticles, enabling the selective aerobic

oxidation of benzyl alcohol under mild conditions. Citrate plays a dual role by regulating nanoparticle dispersion through strong metal–support interactions and by enhancing catalytic activity and product selectivity toward benzaldehyde using molecular oxygen as the sole oxidant, without added bases or stoichiometric oxidants. The combination of a biocompatible, recyclable support with an efficient heterogeneous catalytic system highlights the potential of citrate-engineered hydroxyapatite as a sustainable platform for selective oxidation chemistry. Although preservation of the metallic Au active sites requires storage under a reducing atmosphere prior to use, the catalytic process itself remains environmentally benign. More broadly, this strategy provides a rational framework for engineering metal–support interfaces to develop efficient and sustainable catalysts for aerobic oxidation reactions.

CRediT authorship contribution statement

Afef Mehri: Writing – original draft, Validation, Methodology, Investigation, Formal analysis, Data curation. **Mohamed Hassen V Baouab**: Project administration, Formal analysis, Validation, supervision.

Studies in humans and animals

This work involves not the use of human blood and not the use of animal' subjects.

Declaration of Competing Interest

The authors declare that they have no known competing financial interests or personal relationships that could have appeared to influence the work reported in this paper.

Appendix A. Supporting information

Supplementary data associated with this article can be found

Data availability

The data supporting the findings of this study are available from the corresponding author upon reasonable request.

References

1. Della Pina C, Falletta E, Prati L, Rossi M (2008) Selective oxidation using gold. Chem Soc Rev 37:2077–2095. https://doi.org/10.1039/b707319b

2. Climent MJ, Corma A, Iborra S (2011) Heterogeneous Catalysts for the One-Pot Synthesis of Chemicals and Fine Chemicals. Chem Rev 111:1072–1133. https://doi.org/10.1021/cr1002084

3. Sheldon RA, Arends IWCE, ten Brink G-J, Dijksman A Green, Catalytic Oxidations of Alcohols

4. Zhang J, Yang J, Li X, et al (2022) Efficient Synthesis of Pharmaceutical Intermediates from Biomass-Derived Aldehydes and Ketones over Robust NixAl Nanocatalysts. ACS Sustainable Chem Eng 10:5526–5537. https://doi.org/10.1021/acssuschemeng.2c00115

5. Issa HM, Mohammed DH (2025) A critical review on the journey of benzoic acid in the pharmaceutical industry from manufacturing processes through various uses to disposal: An environmental perspective. Environ Anal Health Toxicol 40:e2025007-2025000. https://doi.org/10.5620/eaht.2025007

6. Wu X, Zhu L, Zhu C, et al (2019) Catalytic Transformation of Bio-oil to Benzaldehyde and Benzoic Acid: An Approach for the Production of High-value Aromatic Bio-chemicals. Current Green Chemistry 6:135–146. https://doi.org/10.2174/2213346106666190830114619

7. Ju Z, Li M, Chen F-E (2024) Enantioselective synthesis of vicinal diols by an enzymatic approach. Molecular Catalysis 557:113956. https://doi.org/10.1016/j.mcat.2024.113956

8. Synthesis of Schiff Bases of Benzaldehyde and Salicylaldehyde as Anti-inflammatory Agents | Iraqi Journal of Pharmaceutical Sciences. https://bijps.uobaghdad.edu.iq/index.php/bijps/article/view/583. Accessed 24 July 2026

9. Volynets GP, Tukalo MA, Bdzhola VG, et al (2019) Benzaldehyde thiosemicarbazone derivatives against replicating and nonreplicating Mycobacterium tuberculosis. J Antibiot (Tokyo) 72:218–224. https://doi.org/10.1038/s41429-019-0140-9

10. Zhang J, Yang J, Li X, et al (2022) Efficient Synthesis of Pharmaceutical Intermediates from Biomass-Derived Aldehydes and Ketones over Robust NixAl Nanocatalysts. ACS Sustainable Chem Eng 10:5526–5537. https://doi.org/10.1021/acssuschemeng.2c00115

11. Santos CBR, Lobato CC, Ota SSB, et al (2023) Analgesic Activity of 5-Acetamido-2-Hydroxy Benzoic Acid Derivatives and an In-Vivo and In-Silico Analysis of Their Target Interactions. Pharmaceuticals 16:1584. https://doi.org/10.3390/ph16111584

12. You B, Cheng Z, Tian Y, et al (2023) Highly Efficient and Selective Oxidation of Benzyl Alcohol by WO42− Catalyst Immobilized by a Phosphonium-Containing Porous Aromatic Framework. Catalysts 13:1309. https://doi.org/10.3390/catal13091309

13. Carabineiro SAC (2019) Supported Gold Nanoparticles as Catalysts for the Oxidation of Alcohols and Alkanes. Front Chem 7:702. https://doi.org/10.3389/fchem.2019.00702

14. Sankar M, He Q, Engel RV, et al (2020) Role of the Support in Gold-Containing Nanoparticles as Heterogeneous Catalysts. Chem Rev 120:3890–3938. https://doi.org/10.1021/acs.chemrev.9b00662

15. Corma A, Garcia H (2008) Supported gold nanoparticles as catalysts for organic reactions. Chem Soc Rev 37:2096–2126. https://doi.org/10.1039/b707314n

16. Metal Catalysts for Heterogeneous Catalysis: From Single Atoms to Nanoclusters and Nanoparticles | Chemical Reviews | ACS Publications. https://pubs.acs.org/chreay/article/118/10/4981/681297/Metal-Catalysts-for-Heterogeneous-Catalysis-From. Accessed 26 July 2026

17. Gawande MB, Goswami A, Felpin F-X, et al (2016) Cu and Cu-Based Nanoparticles: Synthesis and Applications in Catalysis. Chem Rev 116:3722–3811. https://doi.org/10.1021/acs.chemrev.5b00482

18. Munnik P, de Jongh PE, de Jong KP (2015) Recent Developments in the Synthesis of Supported Catalysts. Chem Rev 115:6687–6718. https://doi.org/10.1021/cr500486u

19. Venugopal A, Scurrell MS (2003) Hydroxyapatite as a novel support for gold and ruthenium catalysts: Behaviour in the water gas shift reaction. Applied Catalysis A: General 245:137–147. https://doi.org/10.1016/S0926-860X(02)00647-6

20. Zhang D, Zhao H, Zhao X, et al (2011) Application of Hydroxyapatite as Catalyst and Catalyst Carrier. Progress in Chemistry 23:687–694

21. Szałaj U, Chodara A, Gierlotka S, et al (2023) Enhanced Release of Calcium Ions from Hydroxyapatite Nanoparticles with an Increase in Their Specific Surface Area. Materials 16:6397. https://doi.org/10.3390/ma16196397

22. Li Y, Wu M, Tan J (2022) Sodium Citrate-assisted Preparation of Hydroxyapatite/Gelatin Nanocomposites. Journal of Ceramics 43:667–673. https://doi.org/10.13957/j.cnki.tcxb.2022.04.014

23. Pillai ZS, Kamat PV What Factors Control the Size and Shape of Silver Nanoparticles in the Citrate Ion Reduction Method?

24. Verma G, Barick KC, Shetake NG, et al (2016) Citrate-functionalized hydroxyapatite nanoparticles for pH-responsive drug delivery. RSC Adv 6:77968–77976. https://doi.org/10.1039/c6ra10659e

25. Clarke CJ, Tu W-C, Levers O, et al (2018) Green and Sustainable Solvents in Chemical Processes. Chem Rev 118:747–800. https://doi.org/10.1021/acs.chemrev.7b00571

26. Aneggi E, Campagnolo F, Segato J, et al (2023) Solvent-free selective oxidation of benzyl alcohol using Ru loaded ceria-zirconia catalysts. Molecular Catalysis 540:113049. https://doi.org/10.1016/j.mcat.2023.113049

27. Nakayama A, Sodenaga R, Gangarajula Y, et al (2022) Enhancement effect of strong metal-support interaction (SMSI) on the catalytic activity of substituted-hydroxyapatite supported Au clusters. Journal of Catalysis 410:194–205. https://doi.org/10.1016/j.jcat.2022.04.015

28. Mehri A, Touati H, Kaaroud K, et al (2025) A novel in situ green method for synthesizing a palladium NPs-based catalyst aimed at the selective hydrogenation of aldehydes in cinnamaldehyde. Colloids and Surfaces A: Physicochemical and Engineering Aspects 719:137035. https://doi.org/10.1016/j.colsurfa.2025.137035

29. Thoudam Chanchan Devi, Singh NB, Singh TD (2024) Effect of Citrate on Morphological and Structural Properties of Hydroxyapatite Nanoparticles Synthesized by Wet Chemical Precipitation Method. Colloid J 86:456–465. https://doi.org/10.1134/S1061933X24600027

30. Haruta M (1997) Size- and support-dependency in the catalysis of gold. Catalysis Today 36:153–166. https://doi.org/10.1016/S0920-5861(96)00208-8

31. Heo D, Kim K, Kwon S (2024) Superior Single-Entity Electrochemistry Performance of Capping Agent-Free Gold Nanoparticles Compared to Citrate-Capped Gold Nanoparticles. Nanomaterials 14:1399. https://doi.org/10.3390/nano14171399

32. Lage VD, Brackmann R, Barreto J, et al (2023) CeFe-supported gold active catalyst applied to NO-SCR by CO: Effect of the gold deposition method and pretreatment. Catalysis Communications 181:106732. https://doi.org/10.1016/j.catcom.2023.106732

33. Daniel M-C, Astruc D (2004) Gold Nanoparticles: Assembly, Supramolecular Chemistry, Quantum-Size-Related Properties, and Applications toward Biology, Catalysis, and Nanotechnology. Chem Rev 104:293–346. https://doi.org/10.1021/cr030698+

34. Mangala Gowri V, Panleam T, Giri J, et al (2024) Beyond templates: exploring uncharted territory in anisotropic gold nanostructure-oligomer composites synthesis and electrocatalytic performance towards environmental pollutants. RSC Adv 14:40234–40246. https://doi.org/10.1039/D4RA07744J

35. Sahoo SR, Ke S-C (2021) Spin-Orbit Coupling Effects in Au 4f Core-Level Electronic Structures in Supported Low-Dimensional Gold Nanoparticles. Nanomaterials (Basel) 11:554. https://doi.org/10.3390/nano11020554

36. Đurović MD, Puchta R, Bugarčić ŽD, van Eldik R (2014) Studies on the reactions of [AuCl4]− with different nucleophiles in aqueous solution. Dalton Trans 43:8620–8632. https://doi.org/10.1039/c4dt00247d

37. Swarts JC, Dennis CR, Basson SS (2024) A kinetic study of the reduction of tetrachloroaurate(III) ions by the cyano complexes of iron(II), tungsten(IV) and molybdenum(IV). Reac Kinet Mech Cat 137:673–696. https://doi.org/10.1007/s11144-023-02517-6

38. Pei L, Mori K, Adachi M (2004) Formation Process of Two-Dimensional Networked Gold Nanowires by Citrate Reduction of AuCl 4 - and the Shape Stabilization. Langmuir : the ACS journal of surfaces and colloids 20:7837–43. https://doi.org/10.1021/la049262v

39. Nagy G, Beck A, Sáfrán G, et al (2019) Nanodisperse gold catalysts in oxidation of benzyl alcohol: comparison of various supports under different conditions. Reac Kinet Mech Cat 128:71–95. https://doi.org/10.1007/s11144-019-01615-8

40. Corma A, Garcia H (2008) Supported gold nanoparticles as catalysts for organic reactions. Chem Soc Rev 37:2096–2126. https://doi.org/10.1039/b707314n

41. Sankar M, He Q, Engel RV, et al (2020) Role of the Support in Gold-Containing Nanoparticles as Heterogeneous Catalysts. Chem Rev 120:3890–3938. https://doi.org/10.1021/acs.chemrev.9b00662

42. Fajín JL, Gomes J (2011) Catalytic Reactions on Model Gold Surfaces: Effect of Surface Steps and of Surface Doping. Catalysts 1:40–51. https://doi.org/10.3390/catal1010040

43. Wang L-C, Personick ML, Karakalos S, et al (2016) Active sites for methanol partial oxidation on nanoporous gold catalysts. Journal of Catalysis 344:778–783. https://doi.org/10.1016/j.jcat.2016.08.012

44. Boronat M, Illas F, Corma A (2009) Active Sites for H2 Adsorption and Activation in Au/TiO2 and the Role of the Support. J Phys Chem A 113:3750–3757. https://doi.org/10.1021/jp808271y

45. Gao M, Lyalin A, Takagi M, et al (2015) Reactivity of Gold Clusters in the Regime of Structural Fluxionality. J Phys Chem C 119:11120–11130. https://doi.org/10.1021/jp511913t

46. Raphulu M, McPherson J, Pattrick G, et al (2009) CO oxidation: Deactivation of Au/TiO2 catalysts during storage. Gold Bull 42:328–336. https://doi.org/10.1007/BF03214955

47. Boronat M, Illas F, Corma A (2009) Active Sites for H2 Adsorption and Activation in Au/TiO2 and the Role of the Support. J Phys Chem A 113:3750–3757. https://doi.org/10.1021/jp808271y

48. dos Santos Pereira L, Garcia MA, Rozendo J, et al (2020) Accessing Basic Sites on Modified CoFe2O4 Nanoparticles: Addressing the Selective e 4 Oxidation of Benzyl Alcohol and Unraveling the Au:Pd Ratio Effects by XPS. Journal of the Brazilian Chemical Society. https://doi.org/10.21577/0103-5053.20200075

49. Chen Y, Lim H, Tang Q, et al (2010) Solvent-free aerobic oxidation of benzyl alcohol over Pd monometallic and Au–Pd bimetallic catalysts supported on SBA-16 mesoporous molecular sieves. Applied Catalysis A: General 380:55–65. https://doi.org/10.1016/j.apcata.2010.03.026

50. Enache DI, Barker D, Edwards JK, et al (2007) Solvent-free oxidation of benzyl alcohol using titania-supported gold–palladium catalysts: Effect of Au–Pd ratio on catalytic performance. Catalysis Today 122:407–411. https://doi.org/10.1016/j.cattod.2007.01.003

51. Abad A, Concepción P, Corma A, García H (2005) A Collaborative Effect between Gold and a Support Induces the Selective Oxidation of Alcohols. Angewandte Chemie International Edition 44:4066–4069. https://doi.org/10.1002/anie.200500382

52. Abad A, Corma A, García H (2008) Catalyst Parameters Determining Activity and Selectivity of Supported Gold Nanoparticles for the Aerobic Oxidation of Alcohols: The Molecular Reaction Mechanism. Chemistry – A European Journal 14:212–222. https://doi.org/10.1002/chem.200701263

53. Enache DI, Edwards JK, Landon P, et al (2006) Solvent-Free Oxidation of Primary Alcohols to Aldehydes Using Au-Pd/TiO2 Catalysts. Science 311:362–365. https://doi.org/10.1126/science.1120560

54. Haruta M (2003) When Gold Is Not Noble: Catalysis by Nanoparticles. The Chemical Record 3:75–87. https://doi.org/10.1002/tcr.10053

55. Sheldon RA (2017) The E factor 25 years on: the rise of green chemistry and sustainability. Green Chem 19:18–43. https://doi.org/10.1039/c6gc02157c

56. Sheldon RA (2018) Metrics of Green Chemistry and Sustainability: Past, Present, and Future. ACS Sustainable Chemistry and Engineering 6:32–48. https://doi.org/10.1021/acssuschemeng.7b03505

57. Emeji I, Kumi M, Meijboom R (2024) Performance Evaluation of Benzyl Alcohol Oxidation with tert -Butyl Hydroperoxide to Benzaldehyde Using the Response Surface Methodology, Artificial Neural Network, and Adaptive Neuro-Fuzzy Inference System Model. ACS Omega 9:. https://doi.org/10.1021/acsomega.4c02174

Supplementary Files

This is a list of supplementary files associated with this preprint. Click to download.

- Supplementarymaterial.docx